Hyperfine Interactions (2021) 242: 51
https://doi.org/10.1007/s10751-021-01781-z

^{57}Fe Mössbauer study of $CoCr_xFe_{2-x}O_4$ nano ferrite

P. Tiwari[1] · R. Verma[1] · S. S. Modak[2] · V. R. Reddy[3] · F. Mazaleyrat[4] · S. N. Kane[1]

Accepted: 24 November 2021 / Published online: 6 December 2021

Abstract
We report sol gel auto-combustion synthesized $CoCr_xFe_{2-x}O_4$ ($x = 0.0 - 1.0$) spinel ferrites, and use x-ray diffraction 'XRD', magnetic measurements, and Mössbauer spectroscopy to study the effect of Cr-content on their structural properties, magnetic properties, and correlation between them. Formation of single-phase nono spinel ferrite (grain size: 18.1 – 46.6 nm), is confirmed by XRD. Results show that with increasing Cr-content, lattice parameter decreases, and Cr^{3+} ions remain more populated on B-site, whereas Co^{2+} ions remains almost equally populated on both A, B site, show lower disorder, and modification of A–O – A, B– O – B, A–O – B super-exchange interaction. For Cr-content ≥ 0.75, Mössbauer measurements show presence of a non-magnetic doublet, and isomer shift values confirm that Fe has 3 + oxidation state. Observed structural changes, lead to reduction of saturation magnetization, coercivity.

Keywords Spinel ferrites · XRD · Cationic distribution · Magnetic properties · Mössbauer spectroscopy

1 Introduction

Spinel nanoferrites are focus of research, due to their noteworthy magnetic and structural properties [1]. They can be represented by a general formula AB_2O_4 (*A – divalent metal ion, B – trivalent metal ion*), display face centered cubic (fcc) structure with two inter-penetrating sub-lattices A (*tetrahedral site*) and B (*octahedral site*). Site A, B are respectively

This article is part of the Topical Collection on *Proceedings of the International Conference on the Applications of the Mössbauer Effect (ICAME 2021), 5-10 September 2021, Brasov, Romania*
Edited by Victor Kuncser

✉ S. N. Kane
kane_sn@yahoo.com

[1] Magnetic Materials Laboratory, School of Physics, D. A. University, Khandwa road, Indore 452001, India

[2] Physics Department, Jaypee University of Engineering and Technology, Raghogarh, Guna 473226, India

[3] UGC-DAE Consortium for Scientific Research, Khandwa Road, Indore 452001, India

[4] SATIE, ENS Paris-Saclay, 4 Avenue des Sciences, 91190 Gif-sur-Yvette, France

allocated by divalent; trivalent metal ions, and owing to un-equal magnetic moments on site A, and B, ferrites display spontaneous magnetization [2]. Synthesis protocol [3–5], substitutions and/or presence of various cations [6–9], post-preparation treatments, e.g.: thermal [10, 11]; or no post-preparation thermal treatments [4, 12], ion irradiation [6] etc. play a decisive role in determining their properties. Allocation of ions, and their relative population on A, B site can be used to control magnetic properties of ferrites. Thus, information on cationic distribution facilitate the understanding magnetic properties of spinel nano ferrites [6–9]. Sensible information on cationic distribution can be obtained from x-ray diffraction (XRD) [6, 7, 9, 10], as well as from Mössbauer spectroscopy [13]. XRD data provides structural parameters (e. g. – grain diameter, cationic distribution, inversion parameter, oxygen parameter, dislocation density etc.), while Mössbauer spectroscopy assists in identifying magnetic, non-magnetic phases, to better understand the magnetic properties.

Cobalt ferrite display interesting properties including excellent chemical stability, high Curie temperature, high saturation magnetization, coercivity [14], and have been extensively used in electronic devices, Magnetic Resonance Imaging (MRI) [15, 16], targeted drug delivery, hyperthermia for cancer treatment [5], high density storage devices, magnetic fluids, transformer cores, humidity, and gas sensors, etc. [1, 17]. In Co-ferrite, addition of anti-ferromagnetic Cr^{3+} ions (*Magnetic moment:* $3\mu_B$*, Ionic radius: 0.064 nm*) for ferromagnetic Fe^{3+} ions (*Magnetic moment:* $5\mu_B$*, Ionic radius: 0.067 nm*) would alter the spinel structure, cationic distribution [12], Curie temperature [5, 18], as well as magnetic properties [4, 18, 19]. Thus, Cr^{3+} substitution will modify the structure, and would help in controlling and/or tailoring magnetic properties, and the changes can be effectively probed by XRD, Mössbauer and magnetic studies.

Literature reports synthesis of $CoCr_xFe_{2-x}O_4$ spinel ferrite by sol gel auto-combustion method, with no post-preparation thermal treatment, and shows very similar grain diameter [4, 12]. Sijo [4] clarify that reduction of coercivity, and saturation magnetization is due to variation in magnetic ordering [4]; while Tiwari et al. [12] explain the decrease of saturation magnetization, coercivity respectively in terms of increase of Cr-content, and anisotropy reduction. Panda et al. [19] report Cr-content dependence of structural, magnetic, electrical properties, and explain their variation via changes in particle size, anisotropy, modification of magnetic interactions, and hyperfine parameters. Melikhov et al. [18] report synthesis of $CoCr_xFe_{2-x}O_4$ ferrites by ceramic route, and based on magnetic, Mössbauer studies, explain modification of magnetic properties due to changes in cationic distribution, and anisotropy reduction. With increasing Cr^{3+} content, Mössbauer spectra of $CoCr_xFe_{2-x}O_4$ spinel ferrite, above $x = 0.8$ confirm appearance of a non-magnetic doublet, and an increase of its area [11], along with a magnetic sextet [3, 7]. Krieble et al. [3] report synthesis of $CoCr_xFe_{2-x}O_4$ ($x = 0.0 - 0.8$) ferrite via ceramic technique, and Mössbauer study shows Cr-content dependence of hyperfine field, and preference of Cr on B-site, replacing Fe^{3+} ions, and pushes Co^{2+} ions to A-site. Zhang et al. [5] report synthesis of $Zn_{0.54}Co_{0.46}Cr_{0.6}Fe_{1.4}O_4$ ferrite, by hydrothermal method, and show significant decrease of Curie temperature ~ 45.7 °C, relatively low coercivity ~ 174 Oe, low toxicity, and high specific absorption rate ~ 774 W/kg; thus making these spinel ferrites appropriate for self-regulating hyperthermia.

Aforementioned wide-ranging literature [3–5, 12, 18, 19] focuses separately on the influence of Cr addition on structural modification, hyperfine parameters, Curie temperature, magnetic properties, and specific absorption rate for self-regulating hyperthermia. However, a broad investigation on structural properties, magnetic properties, Mössbauer studies connection among them is still lacking and/or less-explored. So, it is important to

perform such a study, to get correlation among structural; properties, magnetic; Mössbauer studies.

Thus, objective of the present work is to synthesize $CoCr_xFe_{2-x}O_4$ ($x = 0.0 - 1.0$) spinel ferrites by sol gel auto-combustion technique, and to study the effect of Cr-content on structural, magnetic properties, connection among them probed via X-ray diffraction 'XRD', magnetic measurements, and Mössbauer spectroscopy.

2 Material synthesis and characterization

$CoCr_xFe_{2-x}O_4$ ($x = 0.0, 0.25, 0.5, 0.75, 1.0$) nano ferrite series was prepared by sol–gel auto-combustion method, by means of AR grade nitrate-citrate precursors [Chromium nitrate ($Cr(No_3)_3.9H_2O$), Cobalt nitrate ($Co(NO_3)_2\ 6H_2O$), Ferric nitrate – ($Fe(NO_3)_2\ 9H_2O$)], citric acid – ($C_6H_8O_7$), in stoichiometric ratio. Precursors were dissolved in 10 ml de-ionized water, and maintaining metal salt to fuel—citric acid (*acts as chelating agent, and fuel*) ratio as 1:1. Solution pH was maintained at 7 by adding Ammonia solution (NH_4OH). Resulting solution was heated at ~ 115 °C in air till the fluffy powder was formed, called as 'as-burnt' powder. As burnt powder was thermally treated in air at 600 °C for 2 h, and was used for structural, Mössbauer, magnetic characterization.

Room temperature XRD measurements were done by CuK_α radiation (wavelength $\lambda = 0.1540562$ nm) by utilizing Bruker D8 diffractometer. Room temperature transmission Mössbauer spectra were recorded in constant acceleration mode using a ^{57}Co:Rh source. Room temperature hysteresis loops were obtained by vibrating sample magnetometer 'VSM', (*Lakeshore Model 7410*) by applying a maximum applied field: $H_{max.} = \pm 1.9$ T.

3 Analysis of the data

XRD data was analyzed to obtain Lattice parameter '$a_{exp.}$' (*making use of (311) reflection*), x-ray density (ρ_{xrd}), specific surface area *(S)*, and Scherrer's grain diameter (D_s), was obtained by broadening of the highest peak: (311). Rietveld refinement software MAUD [20] was used to get full profile XRD analysis, and it validates the formation of single phase fcc spinel phase. Cationic distribution is obtained by XRD peak intensities employing Bertaut method [8, 21]. It gives cationic distribution by matching the computed, and experimental ratios of intensity for: (422), (311), (400), (220) planes. For dissimilar cation distribution on A, B sites, intensity ratio: I(400)/I(422), I(220)/I(400) varies. The best cation distribution amongst the site A and B for which theoretical, and experimental ratios ((I_{hkl}^{obs} and I_{hkl}^{cal}) of the observed, and calculated intensities agree noticeably, is taken to be the right one. Obtained cationic distribution was used to compute Néel magnetic moment 'n_N' (theoretical magnetization at 0 K:'$M_{s(th)}$)', by using the formula: $n_N = M_B - M_A$ in Bohr magneton (μ_B) where M_A, M_B are respectively magnetic moments of A, B-site. Theoretical lattice parameter ($a_{th.}$), bond angles ($\theta_1, \theta_2, \theta_3, \theta_4, \theta_5$), Oxygen position parameter (u), and inversion parameter (δ) were also computed by cationic distribution. Mössbauer spectra were computer fitted by using NORMOS program [22], with either distribution of hyperfine fields or overlapping of two sextets, corresponding to tetrahedral A, B octahedral site, and a non-magnetic doublet to obtain hyperfine parameters. Coercivity (H_c), saturation magnetization (M_s), static magnetic losses, reduced remanence (M_r/M_s) were obtained from

hysteresis measurements. Anisotropy constant (K_1) was calculated by using the expression: $K_1 = [H_c \times M_s] / 0.96$, where M_s – saturation magnetization, H_c – coercivity.

4 Results and discussions

4.1 Structural properties

Figure 1(a) depicts XRD patterns, while inset (Fig. 1a) shows zoom part of 311 reflection showing peak shift, indicating changes in lattice parameter. Rietveld refined full profile XRD analysis, verifies the formation of single phase nanocrystalline (*grain diameter range between 18.1 nm – 46.6 nm*) cubic spinel phase. Figure 1 (b, c, d, e, f) respectively depict Rietveld refined XRD patterns for samples with x = =0.0, 0.25, 0.50, 0.75, 1.0, showing presence of ferrite peaks. Rietveld refined R parameters are called reliability factors, and are shown in Fig. 1 caption, (R_p*: Profile factor,* R_{wp}*: weighted profile factor,* R_{exp}*: expected weighted profile factor, and goodness of fit 'G.O.F =* R_{WP}/R_{EXP}*'*), and are a measure of the agreement between crystallographic model, and the experimental XRD data. Refinements were carried out until convergence was reached, and the value of the GOF is close to 1. Figure 1(g) depicts the Cr-content dependence of experimental lattice parameter ($a_{exp.}$), while inset shows Cr-content dependence of theoretical lattice parameter ($a_{th.}$). Perusal of Fig. 1(g) shows linear decrease of $a_{exp.}$, explained by the fact that smaller Cr-ion (ionic radius: 0.064 nm) is replacing a larger Fe ion (ionic radius: 0.067 nm), thus reducing unit cell dimensions as was also observed in [10]. Corresponding to Fig. 1(g), following fitting expressions, represents the best linear fit: i) $a_{th.} = 0.3818 - 0.0027$ x, and ii) $a_{exp.} = 0.8379 - 0.0027 \times$ are given.

Cr-content dependence of Scherrer's grain diameter (D_s) is shown in Fig. 2(a). Perusal of Fig. 2(a) depicts that D_s decreases with increase of Cr-content (x), as was also seen in literature [4], and can be expressed by following fitting expression (represents the best linear fit): $D_s = 24.47 \times \exp.(-x/0.1641) + 21.89$. Decrease of D_s is attributable to increase of curvature of grain boundary [23, 24], associated with changes in lattice parameter (see Fig. 1a) [23]. Figure 2(b) depicts Cr-content dependence of x-ray density (ρ_{XRD}), shows linear decrease, depicting increase of porosity, and is consistent with earlier study [4]. Figure 2(b) inset reveal increase of Cr-content till $x = 0.25$, then increases sharply, is in agreement with earlier work [8], and shows compositional dependence of specific surface area. Increase of porosity is also responsible for increase of specific surface area (S), and is useful for heterogeneous catalysis. Behavior of Fig. 2(b) can be expressed by following fitting expression, represents the best linear fit: $\rho_{XRD} = 52 - 35.79$ x. Figure 2(c) depicts Cr-content dependence of dislocation density ρ_D (Lines/m^2), calculated using the expression: $\rho_D = 1/D_s^2$, where D_s – Scherrer's grain diameter, shows linear increase with increasing Cr-content, and is described by fitting expression, represented by the best linear fit: $\rho_D = 0.56 + 2.18$ x, and would have influence on magnetic properties.

Table 1 depicts cationic distribution (on *A, B site*); and experimental, theoretical lattice parameter (a_{exp}, a_{Th}). Perusal of Table 1 shows that with increasing Cr-content, occupation of Fe^{3+} ions increases on A-site, and it decreases on B-site, whereas Co^{2+} ions remain almost equally populated on both A, B site, and is consistent with earlier work [9]. Close agreement between $a_{exp.}$, a_{th} implies that the obtained cationic distribution on A, B site is close to actual cationic distribution.

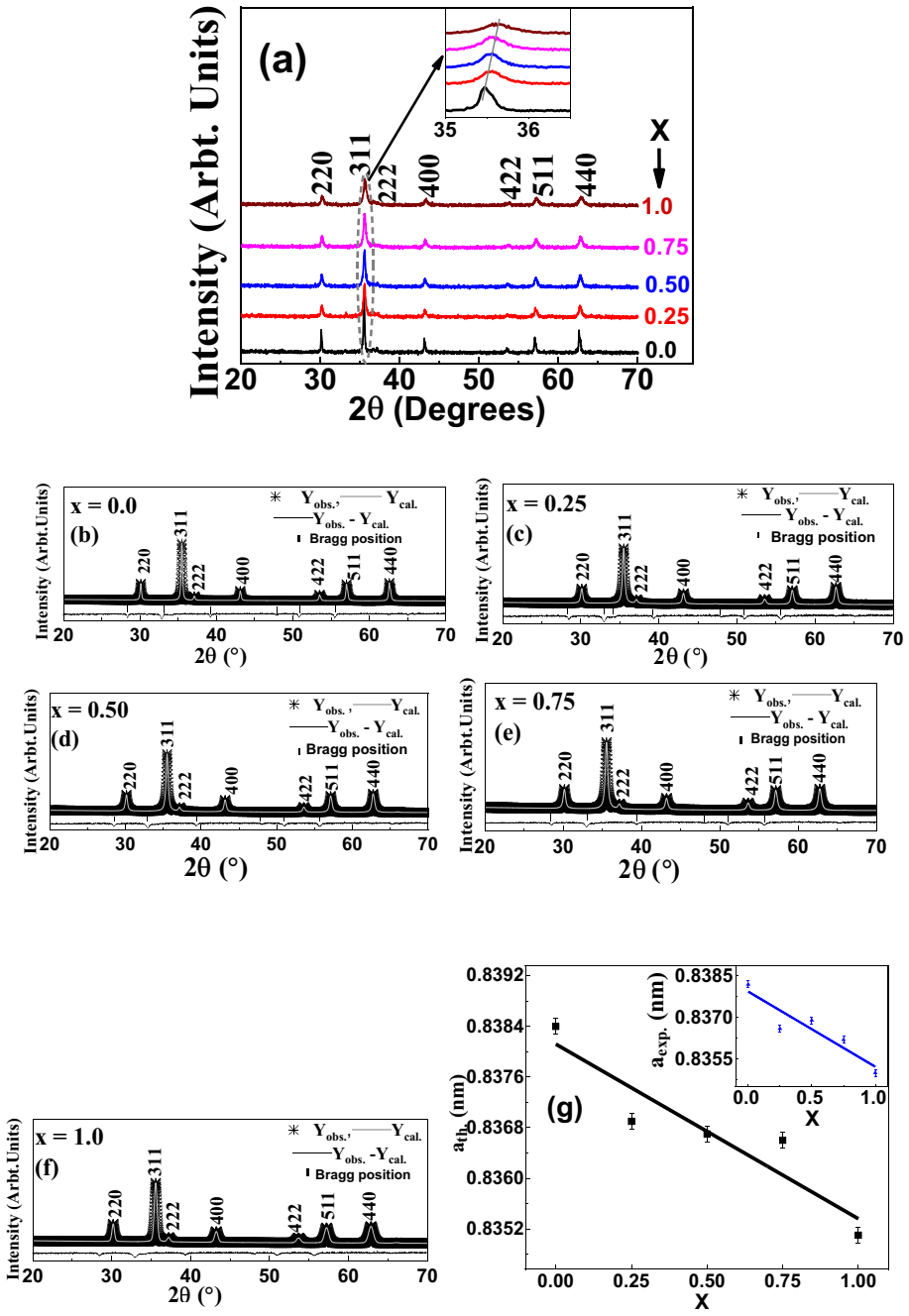

Fig. 1 (**a**) Room temperature XRD patterns of the studied $CoCr_xFe_{2-x}O_4$ ferrites, Inset: shows zoom part of 311 reflection showing peak shift, (**b, c, d, e, f**) Rietveld refined XRD patterns for x = 0.0 (R_p = 7.07%, R_{wp} = 9.01%, R_{exp} = 7.98, G.O.F = 1.13), x = 0.25 (R_p = 6.62%, R_{wp} = 8.48%, R_{exp} = 8.05%, G.O.F = 1.13), x = 0.50 (R_p = 6.66%, R_{wp} = 8.38%, R_{exp} = 8.05%, G.O.F = 1.02), x = 0.75 (R_p = 7.58%, R_{wp} = 9.58%, R_{exp} = 8.62%, G.O.F. = 1.11), x = 1.0 (R_p = 7.58%, R_{wp} = 9.57%, R_{exp} = 8.63, G.O.F = 1.11), (**g**) Cr^{3+} dependent $a_{th.}$ Inset: Cr^{3+} dependent $a_{exp.}$ Continuous lines are linear fit to the data

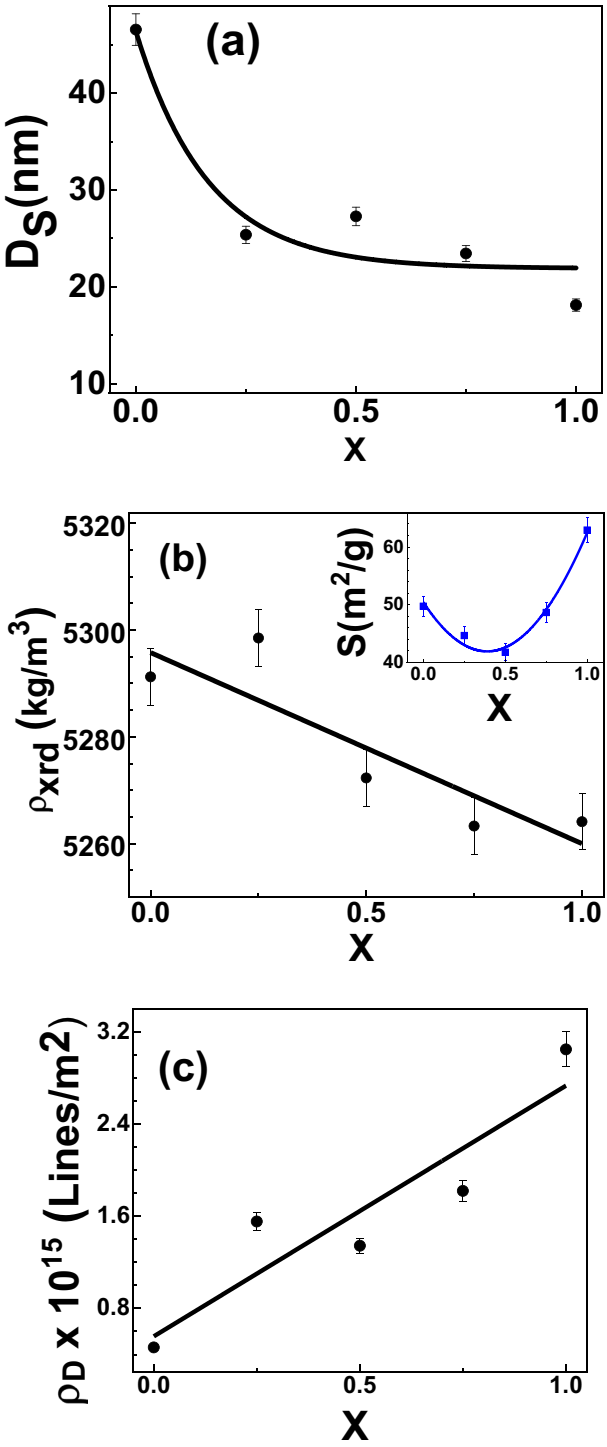

Fig. 2 Cr^{3+} content dependence of: (**a**) Scherrer's grain diameter D_s, (**b**) x-ray density ρ_{xrd}, Inset: Cr^{3+} (x) dependent specific surface area ***S***, (**c**) dislocation density ρ_D

Table 1 Variation of Cation distribution (*for A, B site*), experimental, theoretical lattice parameter (a_{exp}, a_{Th}), of $CoCr_x\ Fe_{2-x}\ O_4$ ferrite as a function of Cr^{3+} content

X	Cation distributions	a_{exp} (nm) (± 0.0024)	a_{Th} (nm) (± 0.0022)
0.0	$(Co^{2+}_{0.75}\ Fe^{3+}_{0.25})^{A}[Co^{2+}_{0.25}\ Fe^{3+}_{1.75}]^{B}$	0.8382	0.8384
0.25	$(Co^{2+}_{0.5}Cr^{3+}_{0.1}Fe^{3+}_{0.4})^{A}[Co^{2+}_{0.5}Cr^{3+}_{0.15}Fe^{3+}_{1.35}]^{B}$	0.8366	0.8369
0.5	$(Co^{2+}_{0.5}Cr^{3+}_{0.1}\ Fe^{3+}_{0.4})^{A}[Co^{2+}_{0.5}Cr^{3+}_{0.4}Fe^{3+}_{1.1}]^{B}$	0.8369	0.8367
0.75	$(Co^{2+}_{0.5}Cr^{3+}_{0.1}\ Fe^{3+}_{0.4})^{A}[Co^{2+}_{0.5}Cr^{3+}_{0.65}\ Fe^{3+}_{0.85}]^{B}$	0.8362	0.8366
1.0	$(Co^{2+}_{0.4}Cr^{3+}_{0.1}Fe^{3+}_{0.5})^{A}[Co^{2+}_{0.6}Cr^{3+}_{0.9}Fe^{3+}_{0.5}]^{B}$	0.8350	0.8351

Figure 3(a) shows the linear decrease of Oxygen position parameter *u*, with inversion parameter, as was also observed in [8, 9]. Observed variation of Oxygen position parameter *u* with inversion parameter is expressed by following equation, showing best linear fit: $u = 0.38 - 0.003\ \delta$. Oxygen positional parameter *u* (*can be used as a quantitative measurement of oxygen displacement*) range between 0.3836 – 0.3835, which is higher than its ideal value: 0.375 [2], reveal enhanced disorder with respect to ideal spinel structure, and affects magnetic properties [7]. Modification of cationic distribution leads to higher degree of inversion with concurrent lowering of disorder due to the movement of O^{2-} ions, as was also observed in literature in other spinel ferrites e. g. in—[10, 11]. Figure 3(b, c) respectively depicts linear decrease of oxygen parameter *u*; and linear increase of inversion parameter with Cr-content. Using Fig. 3(b, c) following fitting expressions (showing best linear fit) can be written: i) $u = 0.38 - 7.2 \times 10^{-4} \times$ and ii) $\delta = 0.29 + 0.2$ x, shows dependence of oxygen parameter *u*, inversion parameter δ on Cr-content (x).

Compositional dependence of bond angles is depicted in Fig. 4. Bond angles are closely related to the strength of A-O-B, B-O-B and, A-O-A super-exchange interaction [25]. Thus, with increasing Cr-content (x), gradual increase of (θ_1, θ_2 θ_5) suggests strengthening of A-O-B, A-O-A interaction through concurrent decrease of (θ_3, θ_4) suggests weakening of B–O–B interaction, and would mirror in determining theoretical magnetic moment $M_{s(th.)}$ *at 0 K*, or n^N_B, as well as saturation magnetization '$M_{s(exp.)}$', as was also reported in literature [7–9].

4.2 Magnetic behavior

Hysteresis loops (see Fig. 5) of the studied samples with varying Cr-content, show variation of saturation magnetization. Inset of Fig. 5 shows increase of saturation magnetization '$M_{s(exp.)}$' with increasing Fe^{3+} ions on B site, is consistent with Néel two sub-lattice model [2, 26], and can be expressed by fitting expression, represents best linear fit: $M_{s(exp.)} = 43.81$ [Fe^{3+} ions on B-site] $- 8.44$.

Figure 6(a-e) respectively depicts Cr-content dependence of coercivity (H_c), anisotropy (K_1), static losses, saturation magnetization: '$M_{s(exp.)}$', theoretical magnetic moment $M_{s(th.)}$ at 0 K, and M_r/M_s. Figure 6(a), (c) shows decrease of H_c, losses, and display better soft magnetic behavior, is consistent with observed lower disorder (see Fig. 3b), and is attributed to decrease of anisotropy (Fig. 6b), as was also reported in earlier studies [12, 18, 19]. It is worth noting that with increasing Cr-content (x), dislocation density (see Fig. 2c) increases, however it does not appear to be very effective to hinder the domain wall movement, thus better soft magnetic behavior is observed, as

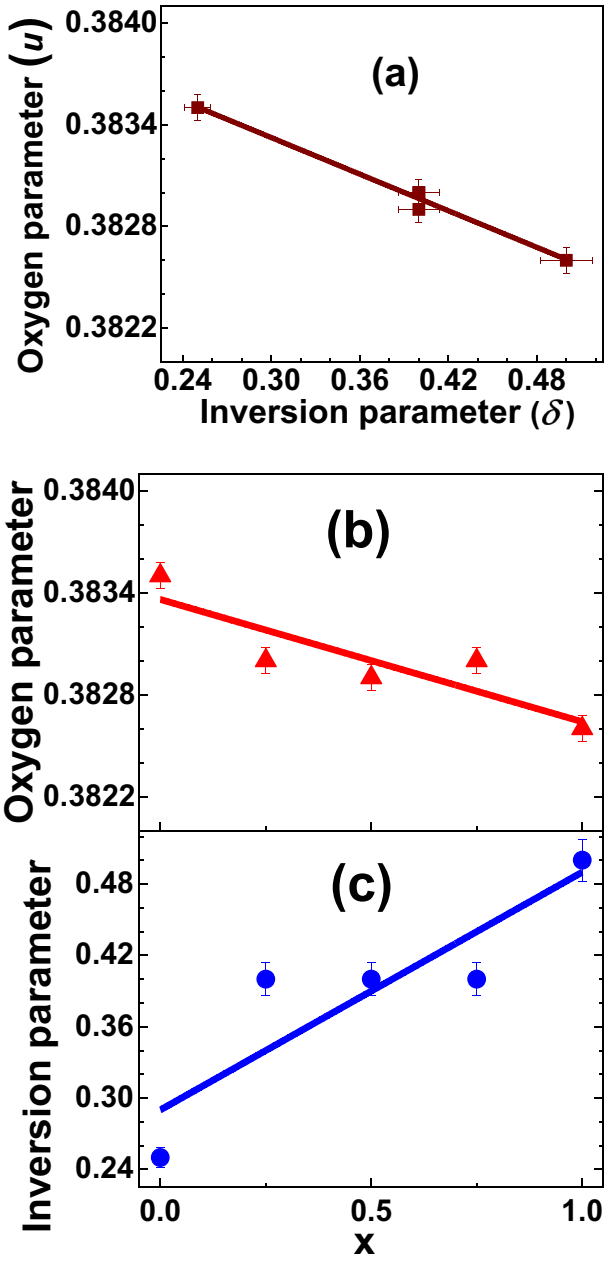

Fig. 3 (**a**) Variation of oxygen parameter u with inversion parameter δ. Cr^{3+} dependence of: (**b**) oxygen parameter u, (**c**) inversion parameter δ. Continuous lines are linear fit to the data

was also observed in [27]. Inset of Fig. 6(a) shows linear dependence of H_c on Scherer's grain diameter (D_s) implies that the studied samples lie in the overlap region between multiple domains or a single domain [25]. Figure 6(b) shows that, anisotropy decreases, as Cr-content increases, can be explained on the basis of single-ion model. According to single-ion model [18], presence of Co^{2+} ions on octahedral (B) site of the spinel ferrites,

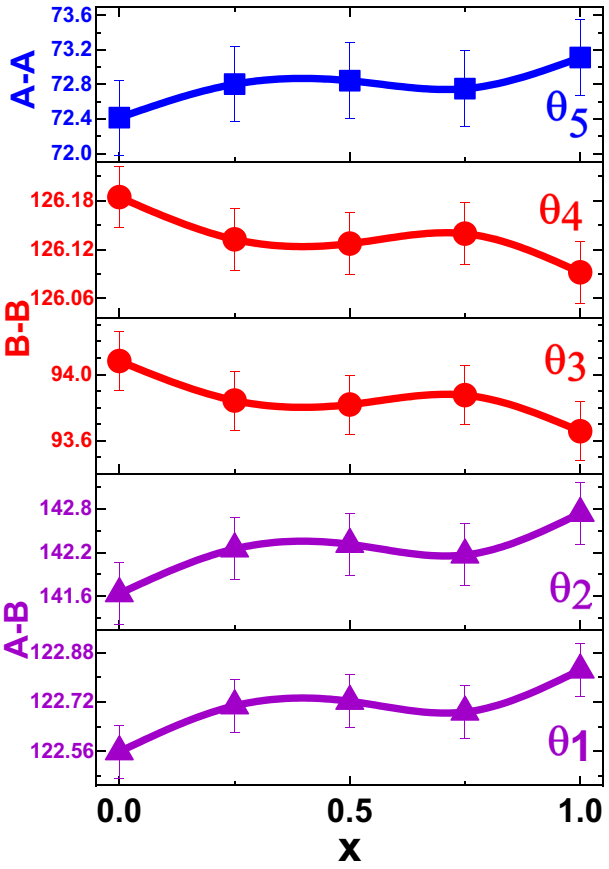

Fig. 4 Compositional dependence of bond angles (θ_1, θ_2, θ_3, θ_4, θ_{5j}. Line connecting points are guide to the eye

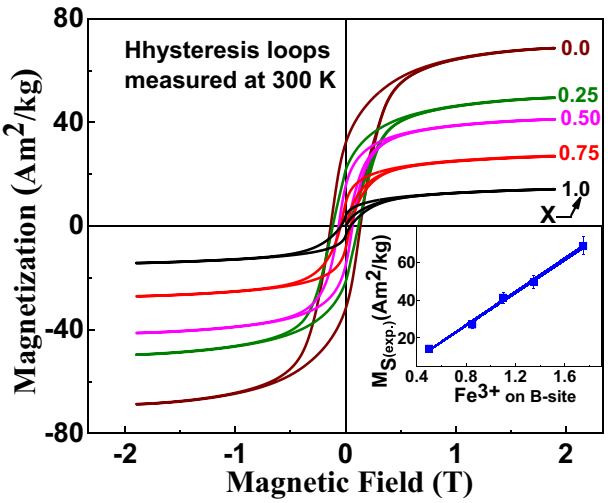

Fig. 5 Hysteresis loops of the studied samples. Inset variation of $M_{s\ (exp.)}$ with of Fe^{3+} ions on B site

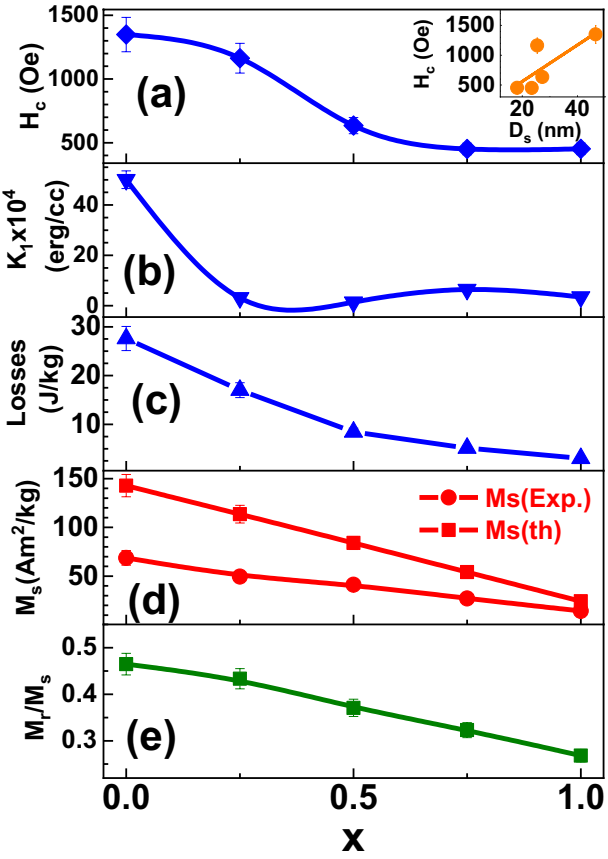

Fig. 6 Cr-content dependence of: (**a**) coercivity H_c, inset: H_c dependence on Schereer's grain diameter D_s, (**b**) anisotropy constant K_1, (**c**) Losses, (**d**) theoretical magnetization at 0 K: $Ms_{(Th.)}$ and experimental saturation magnetization at 300 K $M_{s(exp.)}$, (**e**) reduced remanence M_r/M_s

is accountable for high anisotropy in Co-ferrites. However, addition of Cr^{3+} ions for Fe^{3+} ions, they apparently have a tendency to push Co^{2+} ions to tetrahedral (A-site), and continuous increase of Cr^{3+} ions on B-site (see Table 1), as was also reported in Mössbauer study [3]. Mössbauer results [3] also support the conjuncture that, in general Cr^{3+} ion has a stronger preference to occupy B-site, and to push more Co^{2+} ions to A-site. It is of value to note that with Cr-addition, population of Co^{2+} ions on A, B site remains almost un-changed (see Table 1), which is a different observation as compared to literature, and is ascribable to difference in synthesis protocol. Similar trend of experimental $M_{s(exp.)}$ at 300 K, and that of theoretical magnetization at 0 K: $M_{s(th)}$ shows the applicability of Néel model [26], demonstrating strong correlation between magnetic, structural properties. With increasing Cr-content: i) decrease of $M_{s(exp.)}$ (*as is also observed in* [18]), is ascribable to Cr-content dependent lowering of magnetic ordering [4]; and ii) decrease of $M_{s(th)}$ is attributable to addition of Cr^{3+} ions with lower magnetic moment (*Magnetic moment: 3* μ_B), which are replacing Fe^{3+} ions with higher magnetic moment (*Magnetic moment: 5* μ_B) [4]. Modification of super-exchange interaction *(strengthening of A-O-B, A-O-A interaction with concurrent weakening of B–O–B interaction, as seen in Fig. 4)* is also responsible for the observed decrease of $M_{s(exp.)}$, $M_{s(th)}$ [10, 12]. Obtained M_r/M_s between $0.27-0.47$, indicates variation of inter-grain interaction, and

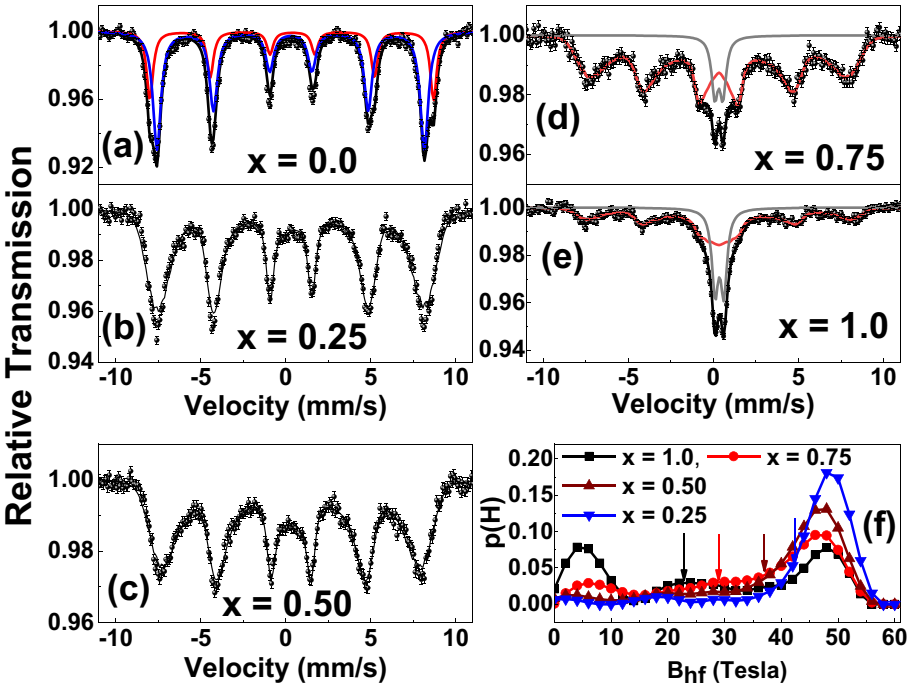

Fig. 7 (**a–e**) Room temperature Mössbauer spectra of the studied samples. Symbols: experimental data, lines: best fit to the experimental data (Sextet: shown in *red, blue color*; Doublet: shown in *gray color*. (**f**) Hyperfine field distribution

Table 2 Mössbauer parameters of the studied $CoCr_xFe_{2-x}O_4$ ferrite samples: B_{hf} – Hyperfine field, I. S. – Isomer shift (*I. S. Values are relative to α-Fe*), Q. S. – quadruple splitting

x	Component (Site)	B_{hf} (T) (±0.1)	I.S.(mm/s) (±0.01)	Q. S. (mm/s) (±0.03)	Width (mm/s) (±0.02)	Area (%) (±2.0)
0.0	Sextet (A)	51.6	0.36	-0.04	0.46	32. 0
	Sextet [B]	48.6	0.29	-0.01	0.57	68. 0
0.25	Sextet	<45.0>	<0.29>	–	0.45	100.0
0.50	Sextet	<39.81>	<0.31>	–	0.45	100.0
0.75	Sextet	<35.07>	<0.32>	–	0.45	89.0
	Doublet	–	0.33	0.48	0.45	11.0
1.0	Sextet	<27.5>	<0.33>	–	0.45	68.0
	Doublet	–	0.36	0.52	0.45	32.0

isotropic behavior of multi-domain particles with no preferred direction of magnetization is also consistent with literature [11, 28].

4.3 Mössbauer spectra

Figure 7(a-e) depict Mössbauer spectra; Fig. 7(f) shows hyperfine field distribution, while Table 2 gives hyperfine parameters. Isomer shift values show that Fe has

3 + oxidation state. Perusal of Table 2 shows Cr-content dependent reduction of internal field on both A, B sites is ascribable to change in the population of Fe^{3+}, Cr^{3+} ions on A, B site. Change in Fe^{3+}, Cr^{3+} ions population on A, B site results in modification of super exchange interaction (see Fig. 4) is consistent with observed decrease of $M_{s(exp.)}$, $M_{s(th)}$ demonstrates correlation between structural, magnetic and Mössbauer data. Area fraction values of (A) and [B] can give Fe ion distribution on A, B site, but presence of paramagnetic doublet for samples with × 0.75 makes it impossible to compute cationic distribution on each site as was also reported in [29]. One can clearly see from the data that with Cr substitution, the lines are becoming broad, and paramagnetic component also increases in intensity as compared to the broad sextet. Because of the broad lines, the Mössbauer data of all the Cr-substituted samples is analyzed with distribution of hyperfine fields. However, the data of sample with $x = 0.0$ is fitted considering two sites. In $CoFe_2O_4$ based systems, instead of internal hyperfine field values, hyperfine field distribution width is considered in assigning the observed sextets to (A), and [B] sites. The site with higher hyperfine field distribution is considered to be due to [B] site [30]. Adopting this method and considering the obtained area fraction values of (A), and [B] sites, the inversion parameter for sample $x = 0.0$ sample is calculated, which is about 0.64 indicating mixed spinel. These results match with the literature, where $CoFe_2O_4$ deviates from inverse spinel [31], when it is prepared with different thermal treatments. Since the Cr substitution is increasing, as expected the average hyperfine is observed to decrease. Since the lines are broad, the identification of (A) and [B] is rather prone to artifacts. However, from the obtained probability distribution of hyperfine field data (see Fig. 7f), one can qualitatively discuss the observations. The probability distribution broadly consists of three features: (i) the dominant peak at about 48 Tesla (*which is more or less at the same position for all the samples*) (ii) peak at low field values (~ 4.5 T), which is growing in intensity with Cr substitution due to increasing paramagnetic component, and (iii) a broad feature, shown by vertical arrows, for all the composition in-between these features. The intermediate feature is clearly seen at a field of about 23 T for $x = 1.0$ sample. Summarizing this: hyperfine field values of two components are such that, the internal field values decreases for the second component, whereas it remains same for the first component. Following the work of Krieble et al. [3, 30], the substituted Cr prefers [B] site, and substitutes Fe^{3+} ions on B-site, and therefore, the internal field values of this site decrease drastically as compared to (A) site, and observations of present study also match with this.

5 Summary and conclusions

Here we summarize the main outcomes of the present work. Cr-addition assisted modification of lattice parameter, cationic distribution shows increase of inversion degree, lowering of disorder, alteration of A–O–A, B–O–B, A–O–B super-exchange interaction, presence of a non-magnetic doublet are collectively accountable for reduction of saturation magnetization, Néel magnetic moment, internal field, at the same time demonstrate better soft magnetic behavior. Thus, present results clearly show the effectiveness of Cr addition in tuning magnetic properties, and have significance for hyperthermia applications for cancer treatment. Although, literature [3, 5, 12, 18, 19] reports composition-assisted dependence of structural properties; magnetic properties, and tuning of Curie temperature for self-regulating hyperthermia etc., however studies on correlation between them are seldom reported

in the literature. Distinctiveness of the present work as compared to literature [3, 5, 12, 18, 19], is that the present work clearly demonstrates strong correlation among structural, magnetic properties, can be recommended to turn magnetic properties via Cr-addition assisted control on structure.

1. Rietveld refined XRD analysis validates the formation of single phase nanocrystalline cubic spinel phase.
2. Decrease of lattice parameter is explained by replacing Fe^{3+} with higher ionic radius by Cr^{3+} with lower ionic radius. Isomer shift values confirm that Fe has 3 + oxidation state.
3. Cr-addition leads to reduction of Fe^{3+} population on B-site, with concurrent increase of Cr^{3+} ion population on B-site, while Co^{2+} ions remains almost equally populated on A, B site.
4. Alteration of cationic distribution shows: increase of inversion degree, lowering of disorder, thus modifies A–O–A, B–O–B, A–O–B super-exchange interaction, presence of a non-magnetic doublet are jointly responsible for reduction of saturation magnetization, Néel magnetic moment, and internal field.
5. Higher Cr-content leads to better soft magnetic behavior, via anisotropy reduction. Linear dependence of coercivity on grain diameter suggests the studied samples lie in the overlap region between multiple-domains or single-domain.
6. Present studies display strong linking between structural, and magnetic properties, and can be recommended to tune magnetic properties via Cr-addition assisted control on structure.

Acknowledgements Authors thank Dr. M. Gupta UGC-DAE CSR, Indore, for doing XRD measurements on the studied samples. SNK acknowledges gratefully for one month 'Invited Professor' stay at ENS Paris-Saclay, Cachan (France) during June 2018.

Author contribution **P. Tiwari**: Preparation of samples, XRD data analysis, **R. Verma**: Preparation of samples, Rietveld refinement of XRD data, **S. S. Modak**: XRD data analysis, **V. R. Reddy**: Mössbauer characterization, data analysis, writing manuscript, **F. Mazaleyrat:** Magnetic characterization, data analysis, writing manuscript. **S. N. Kane**: Conceptualization, Supervision, Resources, preparation of samples, data analysis, writing manuscript. All authors have read and agreed to the submitted version of the manuscript.

Funding This research received no external funding.

Declarations

Consent for publication All authors give their consent for publication of the current manuscript.

Conflict of interests/Competing interests The authors declare that they have no known competing financial interests or personal relationships that could have appeared to influence the work reported in this paper.

References

1. Willard, M.A., Kurihara, L.K., Carpenter, E.E., Calvin, S., Harris, V.G.: Chemically prepared magnetic nanoparticles. Int. Mater. Rev. **49**, 125–170 (2004)
2. Smit, J., Wijn, H.P.J.: Ferrites Philips, p. 137. Eindhoven, Technical Library (1959)
3. Krieble, K., Lo, C.C.H., Melikhov, Y., Snyder, J.E.: Investigation of Cr substitution in Co ferrite $CoCr_xFe_{2-x}O_4$ using Mössbauer spectroscopy. J. Appl. Phys. **99**, 08M912-1-08M912-3 (2006)

4. Sijo, A.K.: Magnetic and structural properties of $CoCr_xFe_{2-x}O_4$ spinels prepared by solution self combustion method. Ceram. Int. **43**, 2288–2290 (2017)
5. Zhang, W., Zuo, X., Niu, Y., Wu, C., Wang, S., Gun, S., Silva, S.R.P.: Novel nanoparticles with Cr^{3+} substituted ferrite for self-regulating temperature hyperthermia. Nanoscale **9**, 13929–13937 (2017)
6. Vucinic-Vasic, M., Bozin, E.S., Bessais, L., Stojanovic, G., Kozmidis-Luburic, U., Abeykoon, M., Jancar, B., Meden, A., Kremenovic, A., Antic, B.: Thermal Evolution of Cation Distribution/Crystallite Size and Their Correlation with the Magnetic State of Yb-Substituted Zinc Ferrite Nanoparticles. J. Phys. Chem. C **117**, 12358–12365 (2013)
7. Lin, J., Zhang, J., Sun, H., Lin, Q., Guo, Z., Yang, H., He, Yun: Structural and magnetic property of Cr^{3+} substituted cobalt ferrite nanomaterials prepared by the sol-gel method. Materials **11**, 2095-1-2095–11 (2018)
8. Raghuvanshi, S., Mazaleyrat, F., Kane, S.N.: $Mg_{1-x}Zn_xFe_2O_4$ nanoparticles: Interplay between cation distribution and magnetic properties. AIP Adv. **8**, 047804–1-047804–11 (2018)
9. Raghuvanshi, S., Tiwari, P., Kane, S.N., Avasthi, D.K., Mazaleyrat, F., Tatarchuk, T., Mironyuk, I.: Dual control on structure and magnetic properties of Mg ferrite: Role of swift heavy ion irradiation. J. Magn. Magn. Mater. **47**, 521–528 (2019)
10. Tiwari, P., Kane, S.N., Deshpande, U.P., Tatarchuk, T., Mazaleyrat, F., Rachiy, B.: Cr content-dependent modification of structural, magnetic properties and bandgap in green synthesized Co–Cr nano-ferrites. Mol. Cryst. Liq. Cryst. **699**, 39–50 (2020)
11. Verma, R., Kane, S.N., Deshpande, U.P., Mazaleyrat, F.: Impact of Cd content on properties of $Ni_{1-x}Cd_xFe_2O_4$ nanoferrites prepared without post-preparation thermal treatment. Mater. Today: Proc. **46**, 2205–2211 (2021)
12. Tiwari, P., Kane, S.N., Verma, R., Mazaleyrat, F.: Synthesis, structural and magnetic properties of CoCrxFe2-rite. AIP Conf. Proc. **2142**, 160016–1-160016-5 (2019)
13. Sawatzky, G.A., Van Der Woude, F., Morrish, A.H.: Mössbauer Study of Several Ferrimagnetic Spinels. Phys. Rev. **187**, 747–757 (1969)
14. Cedeño-Mattei, Y., Perales-Pérez, O., Uwakweh, O.N.C., Xin, Y.: Colossal room-temperature coercivity in size-selected cobalt ferrite nanocrystals. J. Appl. Phys. **107**, 09A741-1-09A741-3 (2010)
15. Na, H.B., Song, I.C., Hyeon, T.: Inorganic nanoparticles for MRI contrast agents. Adv. Mater. **21**, 2133–2148 (2009)
16. Ahmad, T., Rhee, I., Hong, S., Chang, Y., Lee, J.: $NiFe_2O_4$ nanoparticles as contrast agents for magnetic resonance imaging. J. Nanosci. Nanotech. **11**, 5645–5650 (2011)
17. Kharabe, R.G., Devan, R.S., Kanamadi, C.M., Chougule, B.K.: Dielectric properties of mixed Li-Ni-Cd ferrites. Smart Mater. Struct. **15**, N36–N39 (2006)
18. Melikhov, Y., Snyder, J.E., Lo, C.C.H., Matlage, P.N., Song, S.H., Dennis, K.W., Jiles, D.C.: The effect of Cr-substitution on the magnetic anisotropy and its temperature dependence in Cr-substituted cobalt ferrite. IEEE Trans. Magn. **42**, 2861–2863 (2006)
19. Panda, R.K., Muduli, R., Jayarao, G., Sanyal, D., Behera, D.: Effect of Cr^{3+} substitution on electric and magnetic properties of cobalt ferrite nanoparticles. J. Alloys Comp. **669**, 19–28 (2016)
20. Lutterotti, L., Scardi, P.: Simultaneous structure and size-strain refinement by the Rietveld method. J. Appl. Cryst. **23**, 246–252 (1990)
21. Bertaut, E. F. Hebdomadaires C. R.: des Séances de l'Academie des Sciences 230, 213–215 (1950)
22 Brand, R.A.: Improving the validity of hyperfine field distributions from magnetic alloys: Part I: Unpolarized source. Nucl. Instrum. Methods B **28**, 398–416 (1987). https://doi.org/10.1016/0168-583X(87)90182-0
23. Vollath, D.: Nanoparticles – Nanocomposites –Nanomaterials An Introduction for Beginners, p. 30. Wiley-VCH Verlag, Weinheim (2013)
24. Karansky, V.V., Klimov, A.S., Smirnov, S.V.: Structural transformations in Mn–Zn ferrite under low-energy electron beam treatment. Vacuum **173**, 109115-1-109115–6 (2020)
25. Kolhatkar, A.G., Jamison, A.C., Litvinov, D., Willson, R.C., Randall Lee, T.: Tuning the Magnetic Properties of Nanoparticles. Int. J. Mol. Sci. **14**, 15977–16009 (2013)
26. Néel, L.: Aimantation à saturation des ferrites mixtes de Nickel et de Zinc. Comptes Rendus Hebdomadaires Des Seances De L Academie Des Sciences **230**, 375–377 (1950)
27. Kane, S.N., Tiwari, P., Deepti, Verma, R., Deshpande, U.P., Mazaleyrat, F.: Study of structural, magnetic properties and bandgap of spinel $Co_{1-x}Fe_{2+x}O_4$ ferrite. Mater. Today Proc. **32**, 358–364 (2020)
28. Shirsath, S.E., Toksha, B.G., Jadhav, K.M.: Structural and magnetic properties of In^{3+} substituted $NiFe_2O_4$. Mater. Chem. Phys. **117**, 163–168 (2009)

29 Da Silva, S.W., Nakagomi, F., Silva, M.S., Franco, A., Garg, V.K., Oliveira, A.C., Morais, P.C.: Effect of the Zn content in the structural and magnetic properties of $Zn_xMg_{1-x}Fe_2O_4$ mixed ferrites monitored by Raman and Mössbauer spectroscopies. J. Appl. Phys. **107**, 09B503-1-09B503-3 (2010)
30. Krieble, K., Schaeffer, T., Paulsen, J.A., Ring, A.P., Lo, C.C.H., Snyder, J.E.: Mössbauer spectroscopy investigation of Mn-substituted Co-ferrite, $CoMn_xFe_{2-x}O_4$. J. Appl. Phys. **97**, 10F101-1-10F101-3 (2005)
31. Sawatzky, G.A., Van Der Woude, F., Morrish, H.: Cation Distributions in Octahedral and Tetrahedral Sites of the Ferrimagnetic Spinel $CoFe_2O_4$. J. Appl. Phys. **39**, 1204–1206 (1968)